JOURNAL OF SOLID STATE CHEMISTRY 116, 95–102 (1995)

Hydrothermal Syntheses and Properties of New Layered Alkaline Earth Molybdate(VI) Hydrates: Single-Crystal Structure of $BaMo_4O_{13} \cdot 2H_2O$

William T. A. Harrison, Laurie L. Dussack, and Allan J. Jacobson

Department of Chemistry, University of Houston, Houston, Texas 77204-5641

Received June 23, 1994; accepted September 8, 1994

The hydrothermal synthesis, X-ray single crystal structure, and some properties of the new layered $BaMo_4O_{13} \cdot 2H_2O$ are described. (Crystal data: $BaMo_4O_{13} \cdot 2H_2O$, $M_r = 765.11$, orthorhombic, space group *Pbna* (No. 60), $a = 7.680$ (2) Å, $b = 15.756$ (3) Å, $c = 19.689$ (3) Å, $V = 2382.5$ Å^3, $Z = 8$, $R(F) = 4.00\%$, $R_w(F) = 4.39\%$ [3059 reflections with $I > 3\sigma(I)$].) $BaMo_4O_{13} \cdot 2H_2O$ is the first well-characterized barium molybdate hydrate to be reported, and contains three distinct MoO_6 units and an unusual, distorted, MoO_5 group in its layer structure. The 9-coordinate Ba^{2+} cations and water molecules provide the interlayer packing between the $[Mo_4O_{13}]^{2-}$ sheets. $SrMo_4O_{13} \cdot 2H_2O$ has also been prepared, and is isostructural with $BaMo_4O_{13} \cdot 2H_2O$, on the basis of powder X-ray, TGA, and IR data.

INTRODUCTION

Several materials have been previously characterized by single-crystal diffraction in the barium/molybdenum/oxygen phase space. $BaMoO_4$ (1) crystalizes as a typical modification of the ABO_4 scheelite (tetragonal calcium tungstate) structure, and contains tetrahedrally coordinated Mo^{VI} cations. The reduced molybdenum-containing phases $Ba_{0.62}Mo_4O_6$ (2, 3) and $Ba_{1.13}Mo_8O_{16}$ (2) contain Mo in average oxidation states of 2.69 and 3.72 respectively. $Ba_{0.62}Mo_4O_6$ is a distorted modification of $NaMo_4O_6$ (4), contains edge-sharing clusters, and features metal–metal bonding between the molybdenum atoms. $BaMo_6O_{10}$ (5) contains formal Mo^{III} species, but the oxidation states of the four individual molybdenum atoms vary from 2.66 to 3.24, on the basis of bond-length/bond-strength calculations. Mo–Mo metal–metal bonding within the interconnected Mo_6O_{12} clusters is an important structural feature of this phase (5). The newly discovered $Ba_3Mo_{18}O_{28}$ (6) contains 9 different molybdenum atoms, whose oxidation states vary from 2.30 to 3.34 (average = 2.77), based on consideration of Mo–O interactions.

Many other Ba/Mo/O phases have been identified on the basis of X-ray powder diffraction data. $BaMo_3O_{10}$ (7), $BaMo_4O_{13}$ (8), $Ba_3Mo_7O_{24}$ (9), α-$BaMo_2O_7$ (8), β-$BaMo_2O_7$ (9), Ba_2MoO_5 (10), and Ba_3MoO_6 (10) have been reported, but few crystallographic details have been established for these materials. The formal molybdenum oxidation state in all these phases—except in $BaMo_3O_{10}$, where it is 4.67—is Mo^{VI}.

The cubic perovskite-type $BaMoO_3$ (11) (Mo^{IV}) may be prepared by reducing $BaMoO_4$ (1), and recent work suggests that the phase previously written as Ba_2MoO_5 (10, 12) is really $Ba_2Mo_5O_{17}$ (13). The powder patterns of the hydrated barium molybdate(VI) phases $BaMo_3O_{10} \cdot 3H_2O$ (12) and $Ba_8Mo_{20}O_{65}(OH)_6 \cdot 12H_2O$ (14) have been reported, but no unit-cell or structural data were determined. On the basis of these literature X-ray powder data, they are not isostructural with the $BaMo_4O_{13} \cdot 2H_2O$ phase reported here.

Less work has been done on strontium/molybdenum/oxygen/(water) systems. $SrMoO_4$ (15) is isostructural with $BaMoO_4$ (1), and $SrMoO_3$ (16) crystallizes as a typical cubic ABO_3 perovskite-type phase, and is isostructural with $BaMoO_3$ (11). The structure of Sr_3MoO_6 (17) is unknown, but it is not isostructural with Ba_3MoO_6, on the basis of X-ray powder data. Three Sr/Mo/O hydrates have been prepared, $SrMo_3O_{10} \cdot 3H_2O$ (12), $SrMo_3O_{10} \cdot 1\frac{3}{4}H_2O$ (12), and $SrMo_3O_{10} \cdot 4H_2O$ (12), but no crystallographic data have been established for these materials, beyond powder patterns.

In this paper we report the hydrothermal preparation, X-ray single crystal structure, and some properties of $BaMo_4O_{13} \cdot 2H_2O$, a new layered barium molybdate(VI) hydrate. $SrMo_4O_{13} \cdot 2H_2O$ has also been synthesized, and is isostructural with $BaMo_4O_{13} \cdot 2H_2O$, based on powder X-ray, TGA, and IR evidence.

SYNTHESIS AND INITIAL CHARACTERIZATION

Transparent, platy, single crystals (to 2 mm) of $BaMo_4O_{13} \cdot 2H_2O$ were prepared from a reaction mixture

0022-4596/95 $6.00

TABLE 1
X-Ray Powder Data for $BaMo_4O_{13} \cdot 2H_2O$

h k l	d_{obs}(Å)	d_{calc}(Å)	Δd^a	$I_{rel}{}^b$
0 0 2	9.790	9.826	−0.035	22
1 0 1	7.124	7.140	−0.016	4
1 1 1	6.504	6.500	0.004	8
0 2 2	6.141	6.137	0.004	3
1 1 2	5.634	5.640	−0.006	5
1 0 3	4.984	4.979	0.005	27
0 0 4	4.909	4.913	−0.004	18
1 2 2	4.790	4.790	−0.001	8
0 2 4	4.171	4.166	0.005	10
1 3 2	3.961	3.958	0.003	8
2 1 0	3.724	3.723	0.001	19
1 2 4	3.661	3.660	0.001	8
1 0 5	3.499	3.497	0.002	31
1 4 1	3.446	3.442	0.004	4
0 4 3	3.374	3.369	0.004	41
0 0 6	3.275	3.275	0.000	100
2 1 3	3.239	3.236	0.002	17
2 3 0	3.091	3.093	−0.002	9
0 4 4	3.068	3.068	−0.001	25
2 0 4	3.021	3.021	0.000	21
2 1 4	2.961	2.967	−0.006	23
1 5 1	2.880	2.877	0.003	4
0 4 5	2.782	2.779	0.004	4
2 4 1	2.715	2.717	−0.002	4
0 2 7	2.643	2.644	−0.001	15
1 6 1	2.455	2.459	−0.004	18
0 6 3	2.432	2.432	−0.001	8
2 5 1	2.412	2.412	0.000	4
3 1 3	2.356	2.353	0.003	3
1 1 8	2.313	2.314	−0.001	9
2 5 3	2.278	2.278	−0.001	4

[a] $d_{obs} - d_{calc}$.
[b] $100 \times I/I_{max}$.

of initial composition 0.1714 g (0.9 mmol) $BaCO_3$, 0.50 g (3.5 mmol) MoO_3, and 5 ml (0.276 mol)H_2O. Addition of HCl led to evolution of CO_2 and the complete dissolution of the barium phase. The reactants were sealed in a 23-ml capacity, Teflon-lined Parr hydrothermal bomb and heated to 200°C for 3 days. After overnight cooling (final pH = 4.6), the solid products were recovered by vacuum filtration and washing with water. The total yield of air-stable crystals and fines (pass through <170 mesh sieve) was greater than 99% by weight (based on Mo). Systematic initial pH modification (addition of HCl) and reactant-concentration variation revealed little sensitivity of the reaction to these factors, with a 95%+ yield of $BaMo_4O_{13} \cdot 2H_2O$ powder and crystals recovered in all cases.

$SrMo_4O_{13} \cdot 2H_2O$ was prepared from 0.1292 g (0.88 mmol) $SrCO_3$, 0.5 g (3.5 mmol) MoO_3, and 5.0 ml (0.276 mol) water. Addition of HCl resulted in CO_2 loss, and complete solution of the strontium salt. The reactants were heated to 200°C in a 23-ml Parr hydrothermal bomb for 3 days, and cooled overnight (final pH = 3.5). Product recovery, by vacuum filtration and washing with water, produced a quantitative yield of $SrMo_4O_{13} \cdot 2H_2O$ (97%+ by weight, based on Mo), consisting of small, transparent, platy crystals (to 0.1 mm) and white powder. The similarity in X-ray powder patterns of $SrMo_4O_{13} \cdot 2H_2O$ and $BaMo_4O_{13} \cdot 2H_2O$ suggested that the two phases are isostructural.

X-ray powder data for a crushed sample of $BaMo_4O_{13} \cdot 2H_2O$ were recorded on a Scintag XDS 2000 automated powder diffractometer [Cu $K\alpha$ radiation, $\bar{\lambda}$ = 1.54178 Å, T = 25(2)°C]. The instrumental $K\alpha_1/K\alpha_2$ profile was reduced to a single Cu $K\alpha_1$ peak position (λ = 1.540568 Å) by a software "stripping" routine, and d-spacings were established relative to this wavelength. Prior to least-squares minimization of the lattice parameters, hkl-index-to-peak assignments were made on the basis of LAZY-PULVERIX (18) simulations using the single-crystal parameters listed below. Systematic comparison of the observed and calculated I_{hkl} values indicated that was considerable preferred orientation in the [001] direction, perpendicular to the Mo/O layers (*vide infra*). Refined cell-parameter values of a = 7.663 (6) Å, b = 15.716 (9) Å, and c = 19.65 (2) Å (V = 2367 (6) Å^3) resulted. Powder data for $BaMo_4O_{13} \cdot 2H_2O$ are reported in Table 1. Powder X-ray data for $SrMo_4O_{13} \cdot 2H_2O$ were collected and processed using a similar procedure, and refined cell parameters of a = 7.583 (2) Å, b = 15.509 (4) Å, and c = 19.298 (6) Å (V = 2269 (2) Å^3) resulted. X-ray powder data for $SrMo_4O_{13} \cdot 2H_2O$ are listed in Table 2.

The infrared spectrum of $BaMo_4O_{13} \cdot 2H_2O$ powder (KBr pellet method) was recorded between 400 and 4000 cm^{-1} on a Galaxy FTIR 5000 series spectrometer. Characteristic bands due to H_2O stretches (3500–3200 cm^{-1} range and 1601 cm^{-1}) and Mo–O stretches (947, 920, 901, and 797 cm^{-1}) are apparent (Fig. 1a). The IR spectrum of $SrMo_4O_{13} \cdot 2H_2O$ (Figure 1b) is very similar to that of $BaMo_4O_{13} \cdot 2H_2O$, and shows the same characteristic H_2O absorption bands in the 3500–3200 cm^{-1} range and at 1626 cm^{-1}, and Mo–O bands at 922 and 798 cm^{-1}.

Thermogravimetric analysis of $BaMo_4O_{13} \cdot 2H_2O$ (ramp at 3°C/min to 500°C in N_2 atmosphere) revealed a 4.8% weight loss occurring over the temperature range 220–340°C (calc. for complete water loss = 4.7%). Powder X-ray diffraction of the white, post-TGA product heated to 400°C showed a new, complex pattern, unlike that of $BaMo_4O_{13} \cdot 2H_2O$, and also lines due to MoO_3, the latter present as a minor phase. This Ba/Mo/O powder pattern did not match the pattern previously reported for the phase described as anhydrous $BaMo_4O_{13}$ (8), or any other of the barium molybdates noted above. "Autoindexing" attempts were inconclusive. Further heating of this material to 700°C resulted in slow conversion, over several

TABLE 2
X-Ray Powder Data for $SrMo_4O_{13} \cdot 2H_2O$

$h\ k\ l$	d_{obs}(Å)	d_{calc}(Å)	Δd^a	$I_{rel}{}^b$
0 0 2	9.643	9.650	−0.006	47
1 0 1	7.061	7.057	0.004	6
0 0 3	6.425	6.433	−0.008	4
0 2 2	6.047	6.044	0.003	3
1 1 2	5.569	5.565	0.004	4
1 0 3	4.907	4.906	0.002	16
0 0 4	4.825	4.824	0.001	12
1 2 2	4.728	4.726	0.002	6
0 2 4	4.099	4.096	0.003	6
1 3 2	3.903	3.906	−0.003	4
2 1 0	3.681	3.683	−0.002	9
1 2 4	3.606	3.604	0.002	6
0 3 4	3.529	3.527	0.002	3
1 0 5	3.441	3.440	0.002	28
0 4 3	3.320	3.321	−0.001	25
1 4 2	3.251	3.250	0.001	11
0 0 6	3.217	3.216	0.001	100
2 3 0	3.057	3.057	0.000	5
0 4 4	3.022	3.022	0.000	16
2 1 4	2.925	2.927	−0.002	12
0 4 5	2.735	2.735	0.000	4
2 4 1	2.684	2.684	0.000	3
0 2 7	2.598	2.598	0.001	10
0 0 8	2.412	2.412	0.000	6
2 5 1	2.381	2.382	−0.001	2
1 1 8	2.273	2.274	−0.001	4

[a] $d_{obs} - d_{calc.}$
[b] $100 \times I/I_{max}$.

days, to another unidentified Ba/Mo/O phase, and the disappearance of the MoO_3 lines. The powder pattern of this latter phase could not be matched with any previous Ba/Mo/O X-ray data. These phases are being investigated further.

TGA for $SrMo_4O_{13} \cdot 2H_2O$, collected under the same conditions as those used for $BaMo_4O_{13} \cdot 2H_2O$, showed a weight loss of 5.2% over the range 200–390°C (calc. for complete water loss = 5.0%, assuming a stoichiometry of $SrMo_4O_{13} \cdot 2H_2O$). After a powder sample of $SrMo_4O_{13} \cdot 2H_2O$ was heated to 400°C, just above the dehydration point, the greyish product only showed X-ray powder lines due to MoO_3 and $SrMoO_4$ (15), indicating that $SrMo_4O_{13} \cdot 2H_2O$ probably decomposes on dehydration.

Attempts to ion-exchange the barium compound under acidic conditions were unsuccessful, as $BaMo_4O_{13} \cdot 2H_2O$ slowly decomposes in dilute HNO_3 (>0.1 M; pH < 1.2).

CRYSTAL STRUCTURE DETERMINATION

The crystal structure of $BaMo_4O_{13} \cdot 2H_2O$ was determined from single-crystal X-ray diffraction data. A clear, rectangular plate, dimensions ~0.5 × 0.3 × 0.06 mm, was mounted on a thin glass fiber with cyanoacrylate adhesive, and room-temperature [25 (2)°C] intensity data were collected on an Enraf–Nonius CAD4 automated 4-circle diffractometer (graphite-monochromated Mo$K\alpha$ radiation, λ = 0.71073 Å). After 25 strong reflections were located and centered, the unit cell and orientation matrix were established and optimized by least-squares refinement, resulting in the cell parameters listed in Table 3. Excluding intensity standards, 4762 reflections were scanned ($4° < 2\theta < 65°$; $+h, +k, +l$), and the systematic absence conditions in the reduced data ($hk0$, $h \neq 2n$; $h0l$, $h + l \neq 2n$; $0kl$, $k \neq 2n$) uniquely indicated space group *Pbna* nonstandard setting of *Pbcn*, No. 60). An empirical absorption correction (min. = 1.35, max. = 3.07), based on ψ-scans, was applied at the data reduction stage, along with the usual corrections for Lorentz and polarization effects.

The crystal-structure model of $BaMo_4O_{13} \cdot 2H_2O$ was

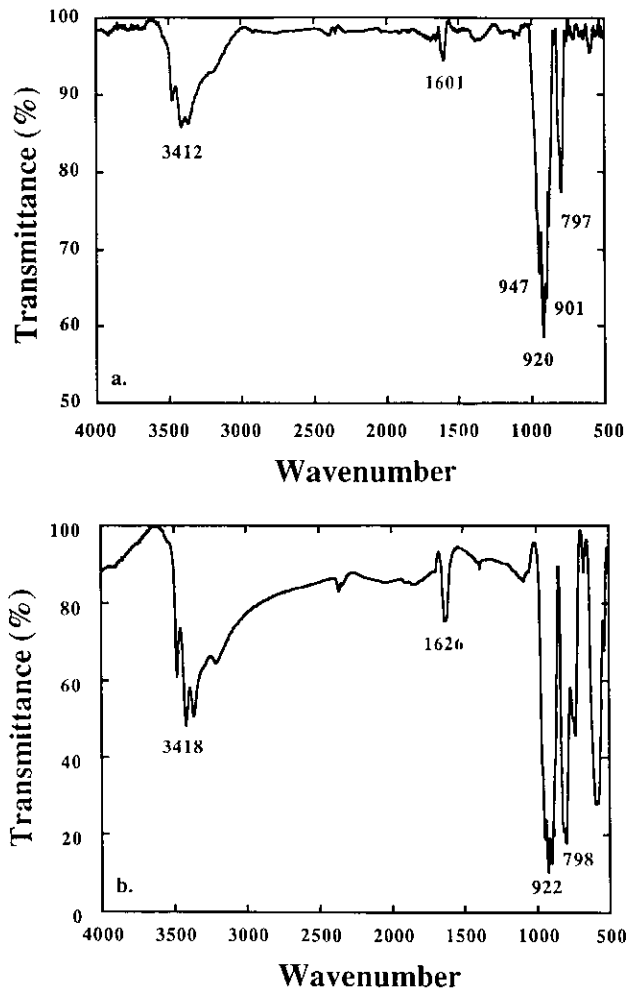

FIG. 1. Infrared spectra for (a) $BaMo_4O_{13} \cdot 2H_2O$, and (b) $SrMo_4O_{13} \cdot 2H_2O$.

TABLE 3
Crystallographic Parameters for $BaMo_4O_{13} \cdot 2H_2O$

Empirical formula	$Ba_1Mo_4O_{15}H_4$
Formula wt.	765.11
Habit	Transparent plate
Crystal size (mm)	0.5 × 0.3 × 0.06
Crystal system	Orthorhombic
a (Å)	7.680 (2)
b (Å)	15.756 (3)
c (Å)	19.689 (3)
V (Å^3)	2382.5
Z	8
Space group	*Pbna* (No. 60)
T (°C)	25 (2)
λ(Mo $K\alpha$) (Å)	0.71073
ρ_{calc} (g/cm^3)	4.266
μ(Mo Kα) (cm^{-1})	73.44
Absorption correction	ψ-scan
Min., max. $\Delta\varrho$ (e/Å^3)	−2.2, 1.8
hkl-data limits	$0 \le 11$, $0 \le 23$, $0 \le 29$
Total data	4762 ($4° < 2\theta < 65°$)
Observed data[a]	3059
Parameters	182
R(F)[b] (%)	4.00
R_w(F)[c] (%)	4.39
S (goodness of fit)	3.06

[a] $I > 3\sigma(I)$ after data merging.
[b] $R = 100 \times \Sigma||F_o| - |F_c||/\Sigma|F_o|$.
[c] $R_w = 100 \times [\Sigma\, w(|F_o| - |F_c|)^2/\Sigma\, w|F_c|^2]^{1/2}$ with w_i as described in the text.

solved and successfully developed in space group *Pbna*. Initial heavy-atom positions (Ba, Mo) were located using the direct-methods program SHELXS-86 (19), and the oxygen-atom positions were located from iterated Fourier difference maps during the refinement. No proton positions could be located from the final difference map, nor could H-atoms be unambiguously placed geometrically. The final cycles of full-matrix least-squares refinement, using complex, neutral-atom scattering factors from the "International Tables" (20), minimized the function $\Sigma\, w_i(F_o - F_c)^2$, and included anisotropic temperature factors and a Larson-type secondary extinction correction (21) [refined value: 27(3)], which corrected for a consistent $F_o < F_c$ effect in strong, low-angle reflections. At the end of the refinement, analysis of the various trends in F_o versus F_c revealed no unusual effects. The least squares, Fourier, and subsidiary calculations were performed using the Oxford CRYSTALS system (22), running on a DEC MicroVAX 3100 computer. Final residuals of R = 4.00% and R_w = 4.34% [Tukey–Prince weighting scheme, fitted with a three-term (Chebyschev polynomial (23)] were obtained. Crystallographic and refinement details are summarized in Table 3. Supplementary tables of anisotropic thermal factors and observed and calculated structure factors are available directly from the authors.

RESULTS

$BaMo_4O_{13} \cdot 2H_2O$ is a new layered structure built up from sheets of vertex- and edge-linked MoO_6 and MoO_5 groups sandwiching barium cations and water molecules. The atomic basis consists of 1 Ba atom, 2 Mo atoms, and 15 oxygen atoms (protons not found), all occupying general crystallographic positions. Final atomic positional and equivalent isotropic thermal parameters for $BaMo_4O_{13} \cdot 2H_2O$ are listed in Table 4, with bond distance and angle data given in Tables 5 and 6, respectively. The Mo/O asymmetric unit and atom-labeling scheme are illustrated in Fig. 2 with ORTEP (24), and the complete crystal structure is shown in Fig. 3.

The crystallographically distinct barium cation in $BaMo_4O_{13} \cdot 2H_2O$ is irregular 9-fold coordinate with respect to nearby oxygen atoms (Fig. 4), including the O-atoms of four different water molecules—O(20), O(20)′, O(21), and O(21)′ (Table 5). The barium cation and water molecules occupy the inter-Mo/O-layer region of the structure, and effectively sandwich the structure in the c-direction, perpendicular to the planes of the $[Mo_4O_{13}]^{2-}$ layers (Fig. 3). A Brese–O'Keefe bond valence sum (BVS) (25) for Ba(1) of 2.36, and a d_{av}(Ba–O) of 2.795 (4) Å result, compared to the expected BVS of 2.00 and ionic-radii sum of 2.82 Å (26) for 9-coordinate Ba^{2+}. The high BVS value for Ba(1) indicates that it is rather "tightly" bonded into the intersheet region, and the thermal parameters for the Ba cation are consequently small.

TABLE 4
Atomic Positional/Thermal Parameters for $BaMo_4O_{13} \cdot 2H_2O$

Atom	x	y	z	U_{eq}[a]
Ba(1)	0.12774 (9)	0.88188 (5)	0.03137 (4)	0.0104
Mo(1)	0.3789 (1)	0.47515 (6)	0.11653 (5)	0.0073
Mo(2)	0.3330 (1)	0.32036 (6)	0.25333 (5)	0.0072
Mo(3)	0.6595 (1)	0.61196 (6)	0.24566 (5)	0.0068
Mo(4)	0.4764 (1)	0.67998 (7)	0.10613 (5)	0.0088
O(1)	0.324 (1)	0.5910 (6)	0.0799 (4)	0.0115
O(2)	0.205 (1)	0.4283 (7)	0.0779 (5)	0.0185
O(3)	0.549 (1)	0.4503 (7)	0.0644 (5)	0.0137
O(4)	0.177 (1)	0.5312 (6)	0.1948 (5)	0.0080
O(5)	0.535 (1)	0.5667 (6)	0.1728 (4)	0.0105
O(6)	0.419 (1)	0.4007 (6)	0.1896 (5)	0.0108
O(7)	0.325 (1)	0.2092 (6)	0.3040 (4)	0.0106
O(8)	0.316 (1)	0.3799 (6)	0.3251 (5)	0.0131
O(9)	0.567 (1)	0.7223 (6)	0.1878 (4)	0.0115
O(10)	0.122 (1)	0.3117 (6)	0.2226 (5)	0.0075
O(11)	0.868 (1)	0.6178 (6)	0.2115 (4)	0.0109
O(12)	0.366 (1)	0.7636 (6)	0.0717 (5)	0.0173
O(13)	0.657 (1)	0.6681 (6)	0.0557 (5)	0.0177
O(20)[b]	−0.086 (1)	0.9559 (7)	−0.0745 (5)	0.0185
O(21)[b]	−0.008 (1)	0.7322 (7)	0.0751 (5)	0.0145

[a] U_{eq} (Å^2) = $(U_1\, U_2\, U_3)^{1/3}$.
[b] Oxygen atom of water molecule.

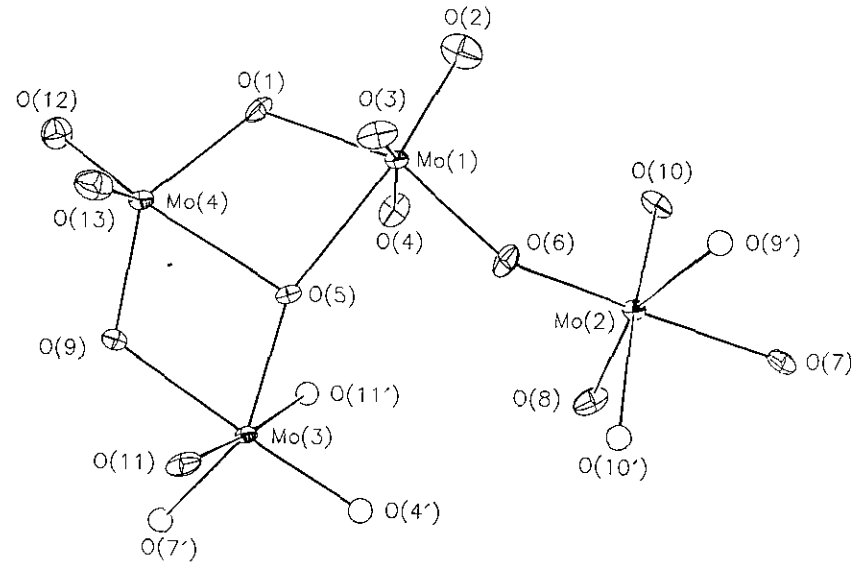

FIG. 2. Asymmetric Mo/O atomic configuration and atom-labeling scheme in $BaMo_4O_{13} \cdot 2H_2O$ (50% thermal ellipses).

Of the four distinct molybdenum cations in the structure, three, Mo(1), Mo (2), and Mo (3), are in distorted octahedral coordination. Mo(1) has two short ($d < 1.75$ Å) "oxo" Mo=O bonds, to O(2) and O(3), not bonded to any other Mo atoms, in typical *cis* configuration, as also found for MoO_3 (27) (Tables 5 and 6). Each of these short Mo=O bonds is *trans* to a long ($d > 2.15$ Å) Mo–O bond. The two remaining Mo–O vertices are intermediate in

TABLE 5
Bond Distances (Å) for $BaMo_4O_{13} \cdot 2H_2O$

Ba(1)–O(1)	2.693 (9)	Ba(1)–O(2)	2.81 (1)
Ba(1)–O(3)	2.784 (9)	Ba(1)–O(8)	2.859 (9)
Ba(1)–O(12)	2.73 (1)	Ba(1)–O(20)	2.90 (1)
Ba(1)–O(20)′	2.71 (1)	Ba(1)–O(21)	2.72 (1)
Ba(1)–O(21)′	2.95 (1)		
Mo(1)–O(1)	2.008 (9)	Mo(1)–O(2)	1.71 (1)
Mo(1)–O(3)	1.707 (9)	Mo(1)–O(4)	2.359 (8)
Mo(1)–O(5)	2.178 (9)	Mo(1)–O(6)	1.881 (9)
Mo(2)–O(6)	1.900 (8)	Mo(2)–O(7)	2.017 (9)
Mo(2)–O(8)	1.701 (9)	Mo(2)–O(9)	2.155 (9)
Mo(2)–O(10)	1.738 (8)	Mo(2)–O(10)′	2.271 (8)
Mo(3)–O(4)	1.736 (9)	Mo(3)–O(5)	1.865 (8)
Mo(3)–O(7)	1.919 (8)	Mo(3)–O(9)	2.198 (9)
Mo(3)–O(11)	1.739 (9)	Mo(3)–O(11)′	2.395 (9)
Mo(4)–O(1)	1.90 (1)	Mo(4)–O(5)	2.262 (9)
Mo(4)–O(9)	1.874 (9)	Mo(4)–O(12)	1.71 (1)
Mo(4)–O(13)	1.71 (1)	Mo(4)–O(7)	2.949 (9)
O(20)–O(2)	3.16 (1)	O(20)–O(2)′	2.88 (1)
O(20)–O(3)	3.17 (1)	O(20)–O(4)	3.12 (1)
O(20)–O(11)	2.94 (1)	O(20)–O(13)	2.80 (1)
O(20)–O(21)	3.01 (1)	O(21)–O(7)	2.78 (1)
O(21)–O(12)	2.92 (1)	O(21)–O(13)	2.79 (1)
O(21)–O(21)′	3.03 (2)		

TABLE 6
Selected Bond Angles (°) for $BaMo_4O_{13} \cdot 2H_2O$

O(1)–Mo(1)–O(2)	93.9 (5)	O(1)–Mo(1)–O(3)	98.8 (4)
O(2)–Mo(1)–O(3)	103.5 (5)	O(1)–Mo(1)–O(4)	75.9 (3)
O(2)–Mo(1)–O(4)	86.4 (4)	O(3)–Mo(1)–O(4)	169.2 (4)
O(1)–Mo(1)–O(5)	72.3 (4)	O(2)–Mo(1)–O(5)	160.8 (4)
O(3)–Mo(1)–O(5)	92.1 (4)	O(4)–Mo(1)–O(5)	77.4 (3)
O(1)–Mo(1)–O(6)	151.1 (4)	O(2)–Mo(1)–O(6)	101.5 (5)
O(3)–Mo(1)–O(6)	101.1 (4)	O(4)–Mo(1)–O(6)	80.9 (4)
O(5)–Mo(1)–O(6)	86.2 (4)		
O(6)–Mo(2)–O(7)	156.3 (4)	O(6)–Mo(2)–O(8)	102.0 (5)
O(7)–Mo(2)–O(8)	93.7 (4)	O(6)–Mo(2)–O(9)	87.6 (4)
O(7)–Mo(2)–O(9)	71.6 (3)	O(8)–Mo(2)–O(9)	156.9 (4)
O(6)–Mo(2)–O(10)	98.4 (4)	O(7)–Mo(2)–O(10)	94.3 (4)
O(8)–Mo(2)–O(10)	105.2 (4)	O(9)–Mo(2)–O(10)	94.0 (4)
O(6)–Mo(2)–O(10)	80.8 (3)	O(7)–Mo(2)–O(10)	82.8 (3)
O(8)–Mo(2)–O(10)	86.2 (4)	O(9)–Mo(2)–O(10)	74.5 (3)
O(10)–Mo(2)–O(10)′	168.4 (4)		
O(4)–Mo(3)–O(5)	106.1 (4)	O(4)–Mo(3)–O(7)	100.1 (4)
O(5)–Mo(3)–O(7)	142.9 (4)	O(4)–Mo(3)–O(9)	162.8 (4)
O(5)–Mo(3)–O(9)	74.8 (3)	O(7)–Mo(3)–O(9)	72.5 (3)
O(4)–Mo(3)–O(11)	103.3 (4)	O(5)–Mo(3)–O(11)	101.2 (4)
O(7)–Mo(3)–O(11)	97.6 (4)	O(9)–Mo(3)–O(11)	93.2 (4)
O(4)–Mo(3)–O(11)	82.0 (4)	O(5)–Mo(3)–O(11)	78.8 (3)
O(7)–Mo(3)–O(11)	79.4 (3)	O(9)–Mo(3)–O(11)	81.3 (3)
O(11)–Mo(3)–O(11)′	174.4 (5)		
O(1)–Mo(4)–O(5)	72.4 (3)	O(1)–Mo(4)–O(9)	136.4 (4)
O(5)–Mo(4)–O(9)	73.1 (3)	O(1)–Mo(4)–O(12)	99.0 (4)
O(5)–Mo(4)–O(12)	159.9 (4)	O(9)–Mo(4)–O(12)	104.4 (4)
O(1)–Mo(4)–O(13)	105.1 (4)	O(5)–Mo(4)–O(13)	95.1 (4)
O(9)–Mo(4)–O(13)	103.8 (4)	O(12)–Mo(4)–O(13)	104.8 (5)
Mo(1)–O(1)–Mo(4)	116.4 (5)	Mo(1)–O(4)–Mo(3)	140.0 (5)
Mo(1)–O(5)–Mo(3)	157.9 (5)	Mo(1)–O(5)–Mo(4)	96.7 (3)
Mo(3)–O(5)–Mo(4)	104.3 (4)	Mo(1)–O(6)–Mo(2)	149.8 (5)
Mo(2)–O(7)–Mo(3)	113.3 (4)	Mo(2)–O(9)–Mo(3)	98.1 (3)
Mo(2)–O(9)–Mo(4)	154.3 (5)	Mo(3)–O(9)–Mo(4)	106.4 (4)
Mo(2)–O(10)–Mo(2)′	146.5 (5)	Mo(3)–O(11)–Mo(3)′	136.2 (4)

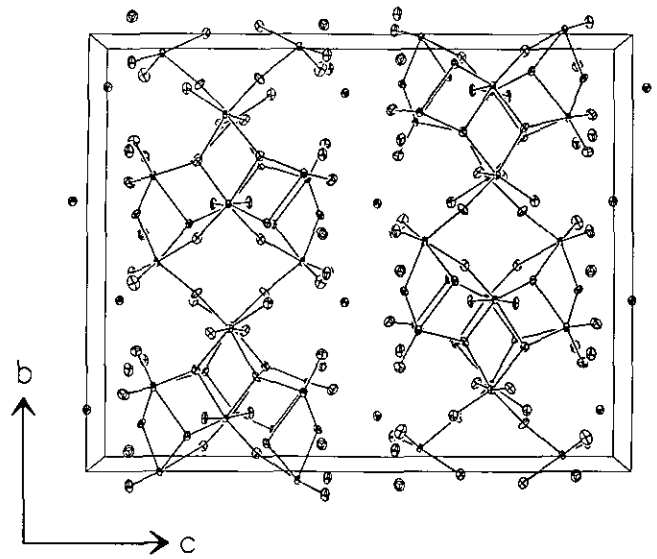

FIG. 3. The crystal structure of $BaMo_4O_{13} \cdot 2H_2O$, viewed down the [100] direction, showing the $[Mo_4O_{13}]^{2-}$ layers separated by barium cations and water molecules (50% thermal ellipses).

length between these extremes, and the average of the six Mo(1)–O bond distances is 1.974(4) Å [ionic-radii sum for Mo^{VI} and O^{-II} = 1.95 Å (26)]. A bond valence sum calculation (25) indicates a BVS of 6.03 for Mo(1), in good agreement with the value of 6.00 expected for Mo^{VI}. Mo(2) has one short oxo Mo=O contact in its coordination sphere, to O(8), and one short Mo(2)=O–Mo′ linkage,

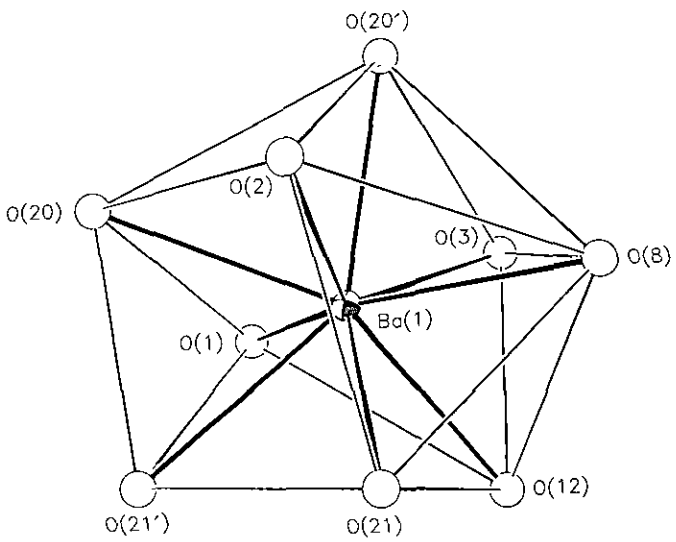

FIG. 4. 9-coordinate Ba(1) coordination polyhedron in $BaMo_4O_{13} \cdot 2H_2O$, with nonbonding O···O contacts <4.0Å indicated by thin lines. O-atoms are represented by spheres of arbitrary radius. O(20), O(20)′, O(21), and O(21)′ are the oxygen atoms of water molecules which occupy the inter-layer region.

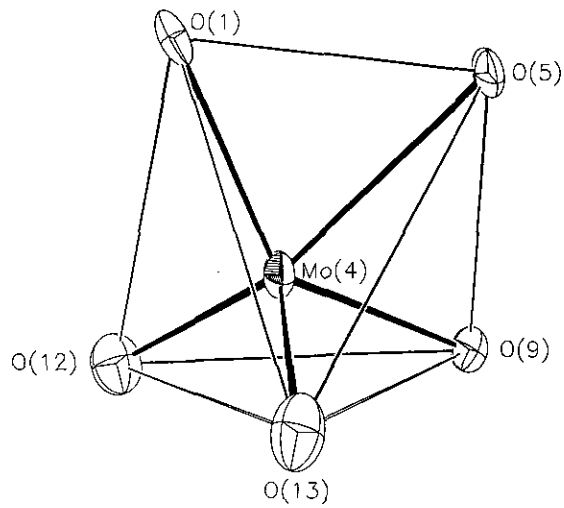

FIG. 5. Mo(4) coordination polyhedron (see text).

to O(10). The *cis* O(8)=Mo(2)=O(10) bond angle is 105.2(4)°. Again, the *trans* Mo–O linkage with respect to each of these two bonds is long, and the two remaining Mo–O vertices are of intermediate length. A d_{av}(Mo(2)–O) of 1.964 (4) Å and a BVS[Mo(2)] of 5.97 result for this molybdenum center. Mo(3) has no uncoordinated Mo=O oxo vertices, but has two short Mo(3)=O–Mo′ bonds, in *cis* configuration, accompanied by long Mo–O bonds *trans* to these two linkages. As observed for Mo(1) and Mo(2), two Mo(3)–O bonds of intermediate length make up the Mo(3) coordination polyhedron, resulting in a d_{av}(Mo(3)–O) of 1.975 (4) Å and a BVS[Mo(3)] of 5.97. The remaining molybdenum atom, Mo(4), is five-coordinate with respect to nearby oxygen atoms (Fig. 5), in distorted square-pyramidal geometry. The Mo=O(12) and Mo=O(13) oxo links are in distorted *cis* conformation (θ[O(12)=Mo(4)=O(13)] = 104.8 (5)°), and a long Mo(4)–O(5) bond (d = 2.262(9)Å) is roughly *trans* to O(12). Two intermediate-length bonds to O(1) and O(9) make up the Mo(4) local coordination: d_{av}(Mo(4)–O) = 1.891 (5) Å, BVS[Mo(4)] = 5.90. There is a very long Mo(4)···O(7) linkage (d = 2.949(9) Å), *trans* to Mo(4)=O(13) (θ[O(13)=Mo(4)···O(7) = 176.8 (4)°), which would complete a distorted "octahedron" of oxygen atoms around Mo(4). Including this Mo(4)···O(7) linkage in the bond-valence-sum calculation for Mo(4) raises its BVS to 5.96.

The oxygen atom coordinations may be summarized as follows: O(2), O(3), O(8), O(12), and O(13) are bonded to just one molybdenum atom; O(1), O(4), O(6), O(7), O(10), and O(11) bridge two Mo centers (θ_{av} = 134°, with a standard deviation of mean = 16°), and O(5) and O(9) make bonds to three nearby Mo atoms, in distorted T-shape coordination. O(20) and O(21) are the oxygen atoms of water molecules and do not make any close Mo–O contacts.

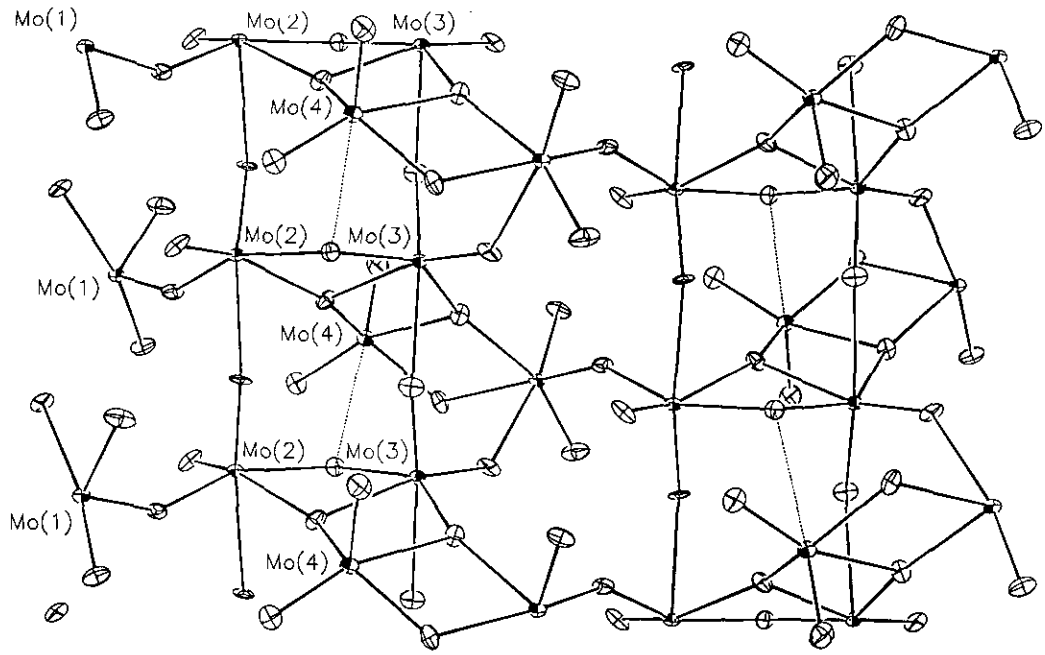

FIG. 6. One $[Mo_4O_{13}]^{2-}$ layer viewed down [001], with selected Mo atoms labelled (50% thermal ellipses). The long Mo(4)···O(7) contact (see text) is indicated by a dotted line.

This Mo/O connectivity leads to the most distinctive feature of the structure of $BaMo_4O_{13} \cdot 2H_2O$—complex, two-dimensional anionic $[Mo_4O_{13}]^{2-}$ layers, which are oriented in the [110] direction (Fig. 6). These sheets are built up from double columns of $Mo(2)O_6$ and $Mo(3)O_6$ octahedra which propagate via Mo(2)=O(10)–Mo(2)′ and Mo(3)=O(11)–Mo(3)′ links in the **a**-direction. Both these infinite linkages contain alternating short and long molybdenum-oxygen bonds, as –Mo=O–Mo=O–Mo=O–, in *trans* configuration. These alternating short-long Mo–O bonds propagate "in phase" in both chains. The Mo(2)- and Mo(3)-centered octahedra share edges via the pair of oxygen atoms O(7) and O(9), which have intermediate Mo–O bond lengths (Table 5). The Mo(2)/Mo(3) double columns are linked into an infinite sheet configuration by Mo(1) octahedra. Each Mo(1) atom links to two Mo(3) atoms in one chain, via Mo(1)–O(5)–Mo(3) and Mo(1)–O(4)–Mo(3) bonds, and to one Mo(2) in an adjacent chain, via a Mo(1)–O(6)–Mo(2) link. Finally, the $Mo(4)O_5$ *unit completes the* $[Mo_4O_{13}]^{2-}$ *layer structure.* Mo(4) shares an edge with the Mo(3) group via O(9) and O(5). These two oxygen atoms are the three-coordinate species noted above. Mo(4) also shares a polyhedral edge with Mo(1), via O(1) and O(5). Alternate Mo(4)-centered groups are located on opposite sides of the Mo(2)/Mo(3) double octahedral chain, and Mo(4)'s two oxo vertices [O(12) and O(13)] point into the interlayer region.

It may finally be noted that the edge-sharing Mo(2)/Mo(3) and Mo(1)/Mo(4) pairs are rather similar in their geometries: each Mo atom has two short oxo-type Mo=O bonds, one of which is *cis*, and one of which is *trans*, to an Mo(2)–O–Mo(3) or Mo(1)–O–Mo(4) octahedral bridging bond. The major difference between the two groupings is the "absent" sixth Mo(4)–O vertex (*vide supra*) accompanied by a long Mo(1)–O(1) bond (d = 2.359 (8) Å), compared to the two long Mo–O bonds (d = 2.271 (8) Å and 2.395 (9) Å) for the equivalent vertices for the Mo(2)/Mo(3) pair (Figs. 7 and 8).

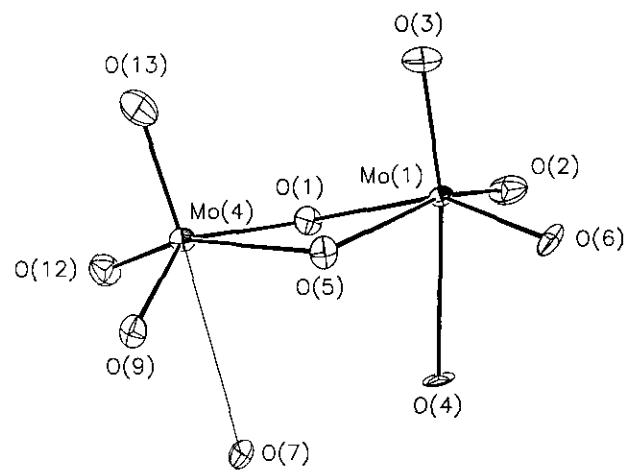

FIG. 7. Detail of the edge-sharing Mo(1)/Mo(4)-centered unit. Compare Figure 8 and the text. The long Mo(4)···O(7) contact is indicated by a thin line (50% thermal ellipses).

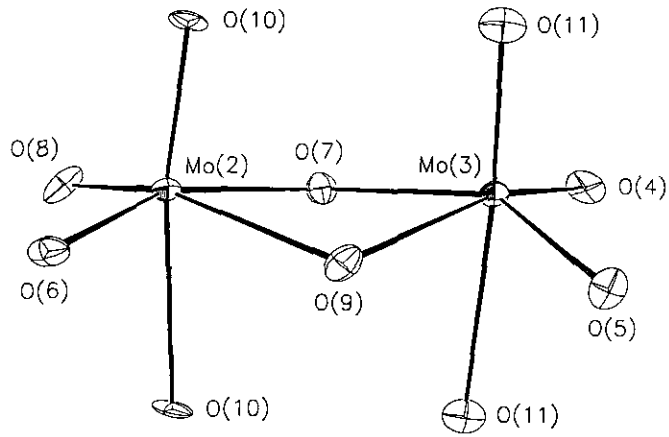

FIG. 8. Detail of the edge-sharing Mo(2)/Mo(3)-centered unit. Compare Figure 7 and the text (50% thermal ellipses).

The similarity in X-ray powder patterns (*vide supra*), in IR spectra (Fig. 1), and in TGA results strongly indicate that $SrMo_4O_{13} \cdot 2H_2O$ is isostructural with $BaMo_4O_{13} \cdot 2H_2O$.

CONCLUSIONS

$BaMo_4O_{13} \cdot 2H_2O$ is the first well-characterized barium molybdate(VI) hydrate, and complements the Ba/Mo/O phases mentioned in the introduction. On the basis of powder X-ray, IR, and TGA evidence, $SrMo_4O_{13} \cdot 2H_2O$ is isostructural with $BaMo_4O_{13} \cdot 2H_2O$. The most interesting structural features of $BaMo_4O_{13} \cdot 2H_2O$ are the complex anionic Mo/O layers built up from distorted octahedral MoO_6 and unusual MoO_5 units. Their corner/edge-shared connectivity is similar to that of molecular polymolybdate anions (28). There is no evidence that any of the molybdenum atoms in $BaMo_4O_{13} \cdot 2H_2O$ are reduced from Mo^{VI}.

ACKNOWLEDGMENTS

We thank Ivan Bernal (University of Houston) for access to X-ray data collection facilities. This work is partially funded by the National Science Foundation (DMR-9214804) and the Welch Foundation.

REFERENCES

1. T. I. Bylichkina, L. I. Soleva, E. A. Pobedimskaya, E. A. Porai-Koshits, and N. V. Belov, *Sov. Phys. Crystallogr.* **15,** 130 (1970).
2. C. C. Torardi and R. E. McCarley, *J. Solid State Chem.* **37,** 393 (1981).
3. C. C. Torardi and R. E. McCarley, *J. Less-Common Met.* **116,** 169 (1986).
4. C. C. Torardi and R. E. McCarley, *J. Am. Chem. Soc.* **101,** 3963 (1979).
5. K. H. Lii, c. C. Wang, and S. L. Wang, *J. Solid State Chem.* **77,** 407 (1988).
6. G. L. Schimek, D. A. Nagaki, and R. E. McCarley, *Inorg. Chem.* **33,** 1259 (1994).
7. M. Haeringer, G. Goldstein, P. Lagrange, and J.-P. Schwing, *Bull. Soc. Chim. Fr.,* 723 (1967).
8. V. M. Zhukovskii, E. V. Tkachenko, and T. A. Rakova, *Russ. J. Inorg. Chem.* **15,** 1734 (1970).
9. O. A. Ustinov, G. P. Novoselov, M. A. Andrianov, and N. T. Chebotarev, *Russ. J. Inorg. Chem.* **15,** 1320 (1970).
10. T. M. Yanushkevich, *Inorg. Mater. USSR* **8,** 1794 (1972).
11. JCPDS Powder Diffraction File, Card 34-323.
12. J. Meullemeestre, *Bull. Soc. Chim. Fr.* (I)236 (1978).
13. JCPDS Powder Diffraction File, Card 38-668.
14. R. Jones, J. M. Adams, and S. Evans, *Mater. Res. Bull.* **22,** 351 (1987).
15. E. Guermen, E. Daniels, and J. S. King, *J. Chem. Phys.* **55,** 1093 (1971).
16. G. Liu, X. Zhao, and H. A. Eick, *J. Alloys Compounds* **187,** 145 (1992).
17. V. M. Zhukovskii, *Russ. J. Inorg. Chem.* **17,** 1481 (1972).
18. K. Yvon, W. Jeitscho, and E. Parthe, *J. Appl. Crystallogr.* **10,** 73 (1977).
19. G. M. Sheldrick, "SHELXS-86 User Guide." Crystallography Department, University of Göttingen, 1986.
20. A. C. Larson, *Acta Crystallogr.* **23,** 664 (1967).
21. "International Tables for X-Ray Crystallography," Vol. IV. Kynoch Press, Birmingham, 1974.
22. D. J. Watkin, J. R. Carruthers, and P. W. Betteridge, "CRYSTALS User Guide." Chemical Crystallography Laboratory, Oxford University, 1985.
23. J. R. Carruthers and D. J. Watkin, *Acta Crystallogr. Sect. A* **35,** 698 (1979).
24. C. K. Johnson, "Report ORNL-5138." Oak Ridge National Laboratory, Oak Ridge, Tennessee, 1976, with local modifications.
25. N. Brese and M. O'Keefe, *Acta Crystallogr. Sect. B* **47,** 192 (1991).
26. R. D. Shannon, *Acta Crystallogr. Sect. A* **32,** 751 (1976).
27. L. Kihlborg, *Ark. Kem.* **21,** 357 (1963).
28. A. F. Wells, "Structural Inorganic Chemistry," 5th ed., p. 516. Oxford Univ. Press, London/New York, 1984.